Thermodynamical stability of calcium borohydride $Ca(BH_4)_2$

Kazutoshi Miwa,[1] Masakazu Aoki,[1] Tatsuo Noritake,[1] Nobuko Ohba,[1] Yuko Nakamori,[2] Shin-ichi Towata,[1] Andreas Züttel,[3,4] and Shin-ichi Orimo[2]

[1]*Toyota Central Research & Development Laboratories, Inc., Nagakute, Aichi 480-1192, Japan*

[2]*Institute for Materials Research, Tohoku University, Sendai 980-8577, Japan*

[3]*Physics Department, University of Fribourg, Perolles, Switzerland*

[4]*Department of Environment, Energy and Mobility, EMPA, Dübendorf, 8600, Switzerland*

(Received 26 June 2006; revised manuscript received 10 September 2006; published 25 October 2006)

We have prepared pure $Ca(BH_4)_2$ without any solvent adducts and determined its structural parameters by powder x-ray diffraction measurement. The crystal structure of $Ca(BH_4)_2$ is found to be orthorhombic with space group *Fddd* (No. 70). Using this structural information, the first-principles calculations have been performed to investigate the fundamental properties of $Ca(BH_4)_2$. The interaction between Ca atoms and BH_4 complexes has an ionic character while the internal bonding of BH_4 is essentially covalent. It is confirmed that $Ca(BH_4)_2$ obeys the linear relationship between the heat of formation and the Pauling electronegativity of the cation, which has been proposed in a previous study [Nakamori *et al.*, Phys. Rev. B **74**, 045126 (2006)].

DOI: 10.1103/PhysRevB.74.155122 PACS number(s): 71.20.Ps, 61.66.Fn, 77.22.−d, 63.20.Dj

I. INTRODUCTION

Complex hydrides have attracted growing interest for hydrogen storage due to their high gravimetric densities of hydrogen. Examples include alanates,[1–4] amides,[5–9] and borohydrides.[10–17] Among borohydrides, alkali borohydrides such as $LiBH_4$ and $NaBH_4$ are well-known and their properties have been studied moderately. Although we can find borohydrides composed of not only alkali metals but also other types of metals in literature,[18,19] little is known for the latter compounds. In this context, we have recently investigated the thermodynamical stability of several metal borohydrides, $M(BH_4)_n$ (M=Li, Na, K, Cu, Mg, Zn, Sc, Zr, and Hf), both theoretically and experimentally.[15] It has been found that the stability of metal borohydrides shows a good correlation with the electronegativity of cations M.

In this paper, we report our study on $Ca(BH_4)_2$. Pure $Ca(BH_4)_2$ without any solvent adducts is prepared and its structural parameters are determined by powder x-ray diffraction measurement. Using this structural information, the first-principles calculations are carried out in order to investigate its fundamental properties. The correlation between the stability of borohydrides and the cation electronegativity proposed in the previous study is examined for $Ca(BH_4)_2$.

II. METHODS

A. Experimental procedure

The starting material for sample preparation is $Ca(BH_4)_2 \cdot 2THF$ (Ref. 20) which has been purchased from Aldrich Co. LTD (product No. 389986). Adduct-free $Ca(BH_4)_2$ is obtained by drawing the THF off under vacuum at 433 K for 1 h. The obtained sample is examined by Raman spectroscopy (JASCO, NRS-3300, 532 nm-laser) and powder x-ray diffractometry (Rigaku, RINT-TTR with Cu $K\alpha$ radiation). The x-ray diffraction data is used to characterize the crystal structure by the Rietveld method using a computer program RIETAN.[21]

B. Computational method

The first-principles calculations have been carried out for $Ca(BH_4)_2$ using the ultrasoft pseudopotential method[22] based on density functional theory.[23] The generalized gradient approximation[24] is adopted for the exchange-correlation energy. For Ca, the 3*s* and 3*p* semicore states are treated as valence. The cutoff energies used in this study are 15 and 120 hartrees for the pseudowave functions and the charge density, respectively. The k-point grids for the Brillouin zone integration are generated so as to make the edge lengths of the grid elements as close to the target value of 0.08 $bohr^{-1}$ as possible. These computational conditions give good convergence for the total energy within 1 meV/atom. The linear response calculation based on density-functional perturbation theory is used to obtain the dielectric properties.[25,26] The phonon eigenmodes are obtained by solving the eigenvalue problem for the dynamical matrix which is calculated by the force-constant method.[27] The computational details can be found in Ref. 14 and the references therein.

III. RESULTS AND DISCUSSION

A. Experiment

Figure 1 shows Raman spectra for prepared $Ca(BH_4)_2$ and purchased $Ca(BH_4)_2 \cdot 2THF$. For comparison purposes, the result measured for pure THF solvent is also indicated. For the purchased sample, Raman modes caused by the THF adduct are clearly observed at around 900 and

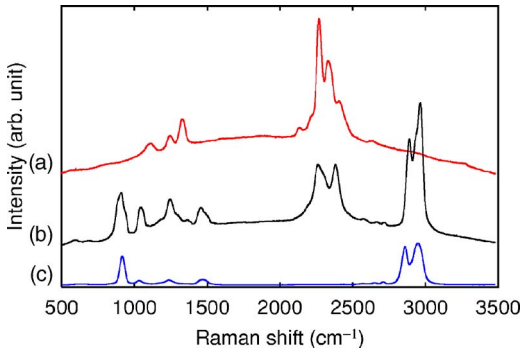

FIG. 1. (Color online) Raman spectra for (a) prepared $Ca(BH_4)_2$, (b) purchased $Ca(BH_4)_2 \cdot 2THF$, and (c) THF solvent.

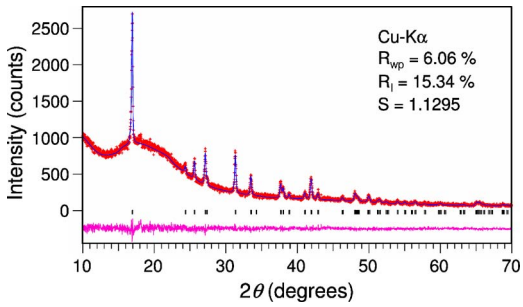

FIG. 2. (Color online) Rietveld analysis pattern for $Ca(BH_4)_2$. The red (+) marks and the blue (upper) line are measured and calculated intensity, respectively, and the purple (bottom) line is the deviation of them. The positions of the Bragg reflections are shown by black bars.

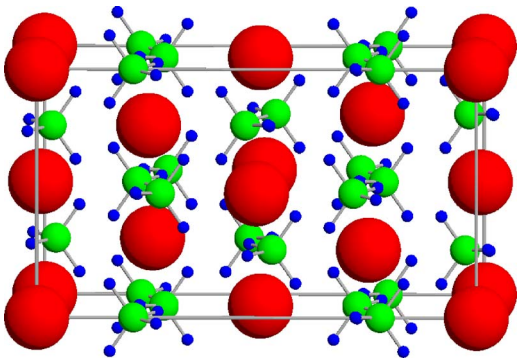

FIG. 3. (Color online) Crystal structure of $Ca(BH_4)_2$. Red (large), green (middle), and blue (small) spheres represent Ca, B, and H atoms, respectively.

2800–3000 cm^{-1}. Other major peaks are found from 2200 to 2500 cm^{-1}, which can be assigned to internal B-H stretching vibrations of BH_4 complexes.[28] On the other hand, Raman modes originated from the THF adduct disappear for the prepared sample, keeping the Raman peaks around 2200–2500 cm^{-1}. This indicates that our purification process successfully removes the THF adduct from the purchase sample. Raman spectra observed at around 1000–1400 cm^{-1} for prepared $Ca(BH_4)_2$ are due to internal B-H bending vibrations of BH_4,[28] which overlap with those of the THF adduct in $Ca(BH_4)_2 \cdot 2THF$.

The Rietveld analysis pattern for prepared $Ca(BH_4)_2$ is shown in Fig. 2. The main peak positions are in good agreement with the previous study.[29] The major feature of this pattern can be interpreted as space group *Fddd* (No. 70) and the calculated pattern fairly reproduces the measured one.[30] Because the intensity of unassigned peaks is very weak, the prepared sample is thought to be almost a single phase of $Ca(BH_4)_2$. The structural parameters obtained by the Rietveld analysis are given in Table I. The B-H bond lengths and the H-B-H bond angles are $d_{B\text{-}H}=1.11-1.13$ Å and $\theta_{H\text{-}B\text{-}H}=102-119°$, respectively. The crystal structure of $Ca(BH_4)_2$ is shown in Fig. 3. As described below, the interaction between Ca atoms and BH_4 complexes has an ionic character. Each metal cation Ca^{2+} is surrounded by six octahedrally coordinated $[BH_4]^-$ anions and each $[BH_4]^-$ has three Ca^{2+} neighbors. Therefore this structure satisfies the electrostatic valence rule.[31]

B. Theoretical predictions

1. Structural property

The structural optimization is performed on $Ca(BH_4)_2$ starting from the experimental geometry, where the atomic positions and the lattice vectors are fully relaxed. Table I also shows the calculated structural parameters. The agreement between the calculated lattice constants and the measured ones is very good. The calculation predicts a nearly ideal tetrahedral shape for BH_4 complexes with $d_{B\text{-}H}=1.23-1.24$ Å and $\theta_{H\text{-}B\text{-}H}=106-113°$. These values are in fairly good agreement with the experimental result mentioned above though the experimental B-H bond lengths are somewhat shorter than the predicted ones. This is probably caused by the experimental difficulty in identifying H positions due to their weak x-ray scattering power.

2. Electronic property

Figure 4 depicts the total and partial densities of states for $Ca(BH_4)_2$. The electronic structure is nonmetallic with a calculated gap of 4.9 eV. The valence states split into two peaks whose positions and widths are quite similar to those of

TABLE I. Structural parameters of $Ca(BH_4)_2$. Space group: *Fddd* (No. 70). The atomic displacement parameters in the experimental results are $B=2.0$, 3.3, 3.8, and 3.8 $Å^2$ for Ca, B, H1, and H2, respectively.

Lattice parameters (Å)	Atom parameters					
		Position	*x*	*y*	*z*	
$a=8.791(1)$	Ca	8*a*	0	0	0	Expt.
$b=13.137(1)$	B	16*f*	0	0.227(4)	0	
$c=7.500(1)$	H1	32*h*	−0.102(16)	0.274(9)	0.037(23)	
	H2	32*h*	0.009(21)	0.176(7)	0.117(16)	
$a=8.802$	Ca	8*a*	0	0	0	Calc.
$b=13.244$	B	16*f*	0	0.2197	0	
$c=7.473$	H1	32*h*	−0.1133	0.2734	0.0132	
	H2	32*h*	0.0020	0.1661	0.1360	

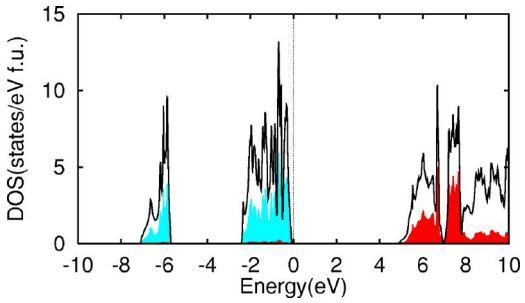

FIG. 4. (Color online) Total and partial densities of states (DOS) for $Ca(BH_4)_2$. The shaded-blue (light) parts indicate the partial DOS for B and H atoms, and the red (dark) parts for the Ca atoms. The origin of energy is set to be the top of valence states.

$LiBH_4$.[14] The valence states are mainly composed of B and H orbitals and the contribution of Ca orbitals is hardly seen. This supports an ionic picture for the interaction between Ca and BH_4.

The valence charge contour plot is shown in Fig. 5(a), where the contributions of the lower eight states composed of Ca semicore states are excluded. The valence charge density around Ca atoms is considerably low. The charge density is strongly localized around $[BH_4]^-$ anions and there are no overlaps between them. In order to visualize the effect of the charge transfer, we also consider the difference between the valence charge density and the superposition of the pseudoatomic charge densities, which is given in Fig. 5(b). The positive regions, in which more electrons are accumulated, are clearly localized around $[BH_4]^-$ anions. However, the negative regions spread over interstitials and no remarkable concentrated regions can be found. This is probably due to a delocalized nature of Ca 4*s* orbitals and might indicate the limitation of the charge density analysis for extended elements.

3. Dielectric property

The dielectric properties are summarized in Table II, which are required to describe the dipole-dipole interactions induced by atomic displacements in the lattice dynamics. The Born effective charge tensor is also useful to consider the bonding characters of materials. The macroscopic high-frequency dielectric permittivity tensor is diagonal because of the orthorhombic symmetry and have small anisotropy. For Ca, the Born effective charge tensor also becomes diagonal due to the site symmetry and their values are fairly close

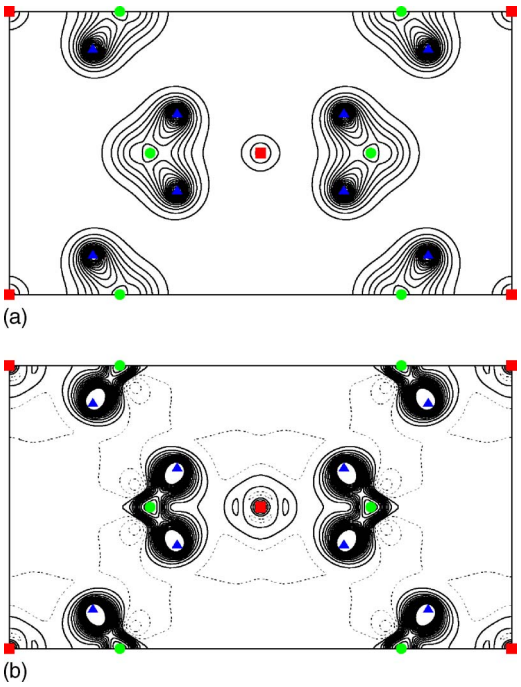

FIG. 5. (Color online) Charge contour plots for $Ca(BH_4)_2$ in the (100) plane. Red squares, green circles, and blue triangles indicate the positions of Ca, B, and H atoms projected on the plane, respectively. (a) The valence charge density excluding the contributions of Ca semicore states. The contour spacing is 0.02 e/bohr^3. (b) The difference between the valence charge density and the superposition of pseudoatomic charge densities, $\rho_{diff}=\rho_{val}-\rho_{atom}$. The contour spacing is 0.004 e/bohr^3 and the dashed contours correspond to negative values. The contours are omitted for $\rho_{diff}>0.06$ e/bohr^3.

to the ideal one of +2. According to the acoustic sum rule, BH_4 complexes are thought to be ionized as $[BH_4]^{-1}$ anions. For B and H, the absolute values of the diagonal elements are small. Since the diagonal elements of Z^*_B are considerably smaller than its nominal charge of +3, the internal bonding of $[BH_4]^-$ is expected to be primarily covalent.

4. Vibrational property

The Γ-phonon frequencies are given in Table III. There are 63 optical Γ-phonon modes because the unit cell contains two formula units. The irreducible representation of them is $7A_g+9B_{1g}+8B_{2g}+9B_{3g}+7A_u+8B_{1u}+7B_{2u}+8B_{3u}$; all *gerade* modes are Raman active, A_u mode is inactive, and other *ungerade* modes are infrared active. The infrared active modes

TABLE II. Dielectric properties of $Ca(BH_4)_2$. Macroscopic high-frequency dielectric permittivity tensors ε_∞ and Born effective charge tensor, Z^*.

	xx	*yy*	*zz*	*xy*	*yz*	*zx*	*xz*	*zy*	*yx*
ε_∞	2.77	2.72	2.62	0	0	0	0	0	0
Z^*_{Ca}	2.43	2.32	2.08	0	0	0	0	0	0
Z^*_B	0.24	0.22	0.22	0	0	±0.01	±0.08	0	0
Z^*_{H1}	−0.53	−0.27	−0.21	±0.21	±0.01	±0.21	±0.13	±0.06	±0.20
Z^*_{H2}	−0.20	−0.42	−0.42	0.00	±0.17	±0.13	±0.14	±0.15	±0.03

TABLE III. Optical Γ-phonon frequencies of $Ca(BH_4)_2$.

Modes		Frequencies (cm^{-1})								
A_g		211	492	1068	1189	1269	2283	2368		
B_{1g}		97	156	257	298	521	1032	1164	2311	2382
B_{2g}		162	245	479	1059	1191	1265	2285	2376	
B_{3g}		43	101	291	339	529	1025	1166	2319	2373
A_u		254	386	1068	1187	1268	2281	2377		
B_{1u}	(TO)	173	216	292	488	1011	1157	2290	2388	
	(LO)	181	243	328	496	1013	1174	2318	2388	
B_{2u}	(TO)	206	406	1056	1178	1266	2281	2355		
	(LO)	296	412	1061	1184	1271	2291	2375		
B_{3u}	(TO)	117	181	295	514	1015	1163	2308	2367	
	(LO)	128	226	340	524	1018	1186	2310	2402	

are divided into the transverse optical (TO) modes and the longitudinal optical (LO) modes due to the dipole-dipole interaction. There are no soft modes, which suggest that the orthorhombic structure determined experimentally is at least metastable, not unstable. As shown in Fig. 6, the Γ-phonon frequencies are classified into three groups. Analyzing the eigenvectors, we confirm that eigenmodes in the regions 1000–1300 cm^{-1} and 2250–2400 cm^{-1} originate from internal B-H bending and stretching vibrations of $[BH_4]^-$ anions, respectively. These frequencies are in good agreement with the Raman spectroscopy measurement for prepared $Ca(BH_4)_2$. The eigenmodes with low frequencies (<550 cm^{-1}) include librational ones which involve the displacements of both Ca^{2+} and $[BH_4]^-$.

5. Heat of formation

The heat of formation for the following reaction is considered, namely, the formation of $Ca(BH_4)_2$ from the elements:

$$\frac{1}{2}\mathrm{Ca} + \mathrm{B} + 2\mathrm{H_2} \rightarrow \frac{1}{2}\mathrm{Ca(BH_4)_2}. \quad (1)$$

We normalize the heat of formation by the number of BH_4 complexes in the formula unit. For the normalized heat of formation ΔH, we have proposed the linear relationship in the previous study,[15]

$$\Delta H = 248.7\chi_P - 390.8. \quad (2)$$

where χ_P is the the Pauling electronegativity of a cation.

The cohesive energies and the zero-point energies (ZPE) for $Ca(BH_4)_2$ and related materials are given in Table IV. For $Ca(BH_4)_2$, the ZPE is estimated from only the Γ-phonon eigenmodes. Since the unit cell contains four BH_4 complexes, the eigenmodes at Γ point involve the effect of the interaction between BH_4 complexes. The Γ-phonon frequencies higher than 1000 cm^{-1} are fairly in good agreement with those of a free $[BH_4]^-$ anion,[28] indicating that the interaction between BH_4 complexes is weak. This justifies the ZPE calculation using only the Γ-phonon frequencies for $Ca(BH_4)_2$. For fcc-Ca, the calculated lattice constant is obtained as $a=5.529$ Å which agrees well with the experimental value of $a=5.58$ Å and the ZPE is calculated using the supercell containing 32 atoms.

From Table IV, the normalized heat of formation is predicted to be $\Delta H=-151$ kJ/mol BH_4 with the ZPE correction. Since $\chi_P=1.0$ for Ca, Eq. (2) gives −142 kJ/mol BH_4 which agrees well with the predicted value in the present study. $Ca(BH_4)_2$ also obeys the linear relationship between ΔH and χ_P. In addition, the ZPE contribution to ΔH is 37 kJ/mol

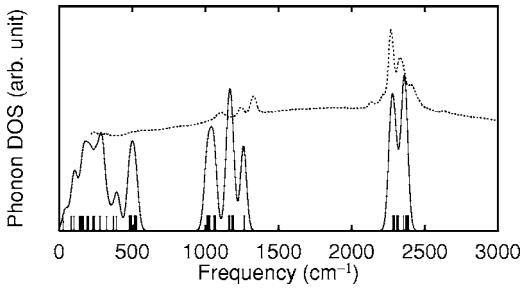

FIG. 6. Phonon density of states for $Ca(BH_4)_2$. The contribution of the Γ-phonon modes indicated by vertical bars is only taken into account and the Gaussian broadening with a width of 30 cm^{-1} is used. The result of Raman spectroscopy measurement for prepared $Ca(BH_4)_2$ is reshown by a dotted line for comparison purposes.

TABLE IV. Cohesive energies E_{coh} (eV/atom) and zero-point energies E_{ZPE} (meV/atom) for $Ca(BH_4)_2$ and related materials. Note that the zero-point energies are not included in E_{coh}.

	E_{coh}	E_{ZPE}
$Ca(BH_4)_2$	3.302	192
Ca	1.845	20
B[a]	6.201	126
H_2[a]	2.272	135
CaH_2	2.694	117
CaB_6	5.987	109

[a]Reference 14.

BH_4 for $Ca(BH_4)_2$. This is close to the approximated value of 33 kJ/mol BH_4 adopted for Eq. (2), which has been estimated using the molecular approximation for a $[BH_4]^-$ anion.

The actual hydrogen desorption reaction for $Ca(BH_4)_2$ will be accompanied with the formation of CaH_2 and/or CaB_6 whose cohesive energies and the zero-point energies are also listed in Table IV. Considering possible combinations of the products, the hydrogen desorption reaction for $Ca(BH_4)_2$ is expected to be

$$Ca(BH_4)_2 \rightarrow \frac{2}{3}CaH_2 + \frac{1}{3}CaB_6 + \frac{10}{3}H_2, \qquad (3)$$

with the enthalpy change of 32 kJ/mol H_2. The theoretical gravimetric density of the effective hydrogen is 9.6 mass%. The thermogravimetric analysis for prepared $Ca(BH_4)_2$ shows that the total mass loss up to 800 K is 9.2 mass%, which supports the overall reaction of Eq. (3). However, this measurement also suggests the existence of an unknown intermediate compound for the reaction of Eq. (3). More detailed investigations are required to determine the reaction pathways and the energetics for the hydrogen desorption reaction of $Ca(BH_4)_2$.

IV. SUMMARY

In summary, we have prepared adduct-free $Ca(BH_4)_2$ and determined its structural parameters experimentally. Using this structural information, the first-principles calculations have been performed to investigate the fundamental properties of $Ca(BH_4)_2$. The linear correlation between the heat of formation and the Pauling electronegativity of the cation, which has been proposed in the previous study,[15] is also held for $Ca(BH_4)_2$. The hydrogen desorption reaction is predicted to be $Ca(BH_4)_2 \rightarrow \frac{2}{3}CaH_2 + \frac{1}{3}CaB_6 + \frac{10}{3}H_2$, which is supported by the thermogravimetric analysis. However, this measurement also suggests the existence of an unknown intermediate compound and more detailed investigations are required for this reaction.

ACKNOWLEDGMENTS

The authors would like to thank M. Matsumoto, H.-W. Li, and S. Hyodo for valuable discussions. This study was partially supported by the New Energy and Industrial Technology Development Organization (NEDO), International Joint Research under the "Development for Safe Utilization and Infrastructure of Hydrogen" Project (2005-2006).

[1] B. Bogdanović and M. Schwickardi, J. Alloys Compd. **253**, 1 (1997).
[2] R. A. Zidan, S. Takara, A. G. Hee, and C. M. Jensen, J. Alloys Compd. **119**, 1 (1999).
[3] L. Zaluski, A. Zaluska, and J. O. Ström-Olsen, J. Alloys Compd. **290**, 71 (1999).
[4] K. J. Gross, S. Guthrie, S. Takara, and G. Thomas, J. Alloys Compd. **297**, 270 (2000).
[5] P. Chen, Z. Xiong, J. Luo, J. Lin, and L. Tan, Nature (London) **420**, 302 (2002).
[6] S. Orimo, Y. Nakamori, G. Kitahara, K. Miwa, N. Ohba, T. Noritake, and S. Towata, Appl. Phys. A: Mater. Sci. Process. **79**, 1765 (2004).
[7] W. Luo, J. Alloys Compd. **381**, 284 (2004).
[8] H. Y. Leng, T. Ichikawa, S. Hino, N. Hanada, S. Isobe, and H. Fujii, J. Phys. Chem. B **108**, 8763 (2004).
[9] Y. Nakamori, G. Kitahara, K. Miwa, S. Towata, and S. Orimo, Appl. Phys. A: Mater. Sci. Process. **80**, 1 (2005).
[10] A. Züttel, P. Wenger, S. Rentsch, P. Sudan, Ph. Mauron, and Ch. Emmenegger, J. Power Sources **118**, 1 (2003).
[11] Y. Kojima and T. Haga, Int. J. Hydrogen Energy **28**, 989 (2003).
[12] G. Renaudin, S. Gomes, H. Hagemann, L. Keller, and K. Yvon, J. Alloys Compd. **375**, 98 (2004).
[13] S. Orimo, Y. Nakamori, G. Kitahara, K. Miwa, N. Ohba, S. Towata, and A. Züttel, J. Alloys Compd. **404-406**, 427 (2005).
[14] K. Miwa, N. Ohba, S. I. Towata, Y. Nakamori, and S. I. Orimo, Phys. Rev. B **69**, 245120 (2004).
[15] Y. Nakamori, K. Miwa, A. Ninomiya, H. Li, N. Ohba, S. Towata, A. Züttel, and S. Orimo, Phys. Rev. B **74**, 045126 (2006).
[16] N. Ohba, K. Miwa, M. Aoki, T. Noritake, S. I. Towata, Y. Nakamori, S. I. Orimo, and A. Züttel, Phys. Rev. B **74**, 075110 (2006).
[17] S. Orimo, Y. Nakamori, N. Ohba, K. Miwa, M. Aoki, S. Towata, and A. Züttel, Appl. Phys. Lett. **89**, 021920 (2006).
[18] E. A. Sullivan and R. C. Wade, *Gravity Concentration to Hydrogen Energy*, Kirk-Othmer Encyclopedia of Chem. Tech. Vol. 12, 3rd ed. (Wiley-Interscience, New York, 1980), p. 772.
[19] http://hydpark.ca.sandia.gov/MaterialsFrame2.html
[20] H. Nöth, Z. Anorg. Allg. Chem. **554**, 113 (1987).
[21] F. Izumi and T. Ikeda, Mater. Sci. Forum **321-324**, 198 (2000).
[22] D. Vanderbilt, Phys. Rev. B **41**, 7892 (1990).
[23] P. Hohenberg and W. Kohn, Phys. Rev. **136**, B864 (1964); W. Kohn and L. J. Sham, Phys. Rev. **140**, A1133 (1965).
[24] J. P. Perdew, K. Burke, and M. Ernzerhof, Phys. Rev. Lett. **77**, 3865 (1996); **78**, 1396(E) (1997).
[25] N. Ohba, K. Miwa, N. Nagasako, and A. Fukumoto, Phys. Rev. B **63**, 115207 (2001).
[26] X. Gonze and C. Lee, Phys. Rev. B **55**, 10355 (1997).
[27] K. Kunc and R. M. Martin, Phys. Rev. Lett. **48**, 406 (1982).
[28] For a free $[BH_4]^-$ anion, a theoretical prediction gives normal mode frequencies of 1029 and 1154 cm^{-1} for B-H bending vibrations and 2225 and 2236 cm^{-1} for B-H stretching ones. See Ref. 14.
[29] N. S. Kedrova and N. N. Mal'tseva, Russ. J. Inorg. Chem. **22**, 973 (1977): No structural parameters are available in this paper.
[30] In the Rietveld analysis, the positions of Ca and B atoms are firstly solved and then structural parameters including hydrogen positions are fully optimized, where H atoms are initially placed at the tetrahedral sites around B atoms and no constraints except for symmetry restriction are applied during the least-squares fitting. We choose two sets of initial hydrogen positions, $[H1(x,y,z)=(-0.1,0.27,0.0),\ H2(x,y,z)=(0.0,0.17,0.1)]$ and $[H1(x,y,z)=(-0.1,0.17,0.0),\ H2(x,y,z)=(0.0,0.27,0.1)]$, but both sets converge with the same parameters shown in Table I.
[31] H. D. Megaw, *Crystal Structures: A Working Approach* (W. B. Saunders Company, Philadelphia, 1973).